Monthly Notices
of the
ROYAL ASTRONOMICAL SOCIETY

MNRAS **461,** 4406–4418 (2016)
Advance Access publication 2016 July 4

doi:10.1093/mnras/stw1577

On the orbital evolution of a pair of giant planets in mean motion resonance

Q. André[1,2]★ and J. C. B. Papaloizou[1]

[1]*DAMTP, University of Cambridge, Wilberforce Road, Cambridge CB3 OWA, UK*
[2]*Département de Physique, ENS Cachan, Université Paris-Saclay, 61 Avenue du Président Wilson, F-94230 Cachan, France*

Accepted 2016 June 30. Received 2016 June 30; in original form 2015 July 9

ABSTRACT

Pairs of extrasolar giant planets in a mean motion commensurability are common with 2:1 resonance occurring most frequently. Disc–planet interaction provides a mechanism for their origin. However, the time-scale on which this could operate in particular cases is unclear. We perform 2D and 3D numerical simulations of pairs of giant planets in a protoplanetary disc as they form and maintain a mean motion commensurability. We consider systems with current parameters similar to those of HD 155358, 24 Sextantis and HD 60532, and disc models of varying mass, decreasing mass corresponding to increasing age. For the lowest mass discs, systems with planets in the Jovian mass range migrate inwards maintaining a 2:1 commensurability. Systems with the inner planet currently at around 1 au from the central star could have originated at a few au and migrated inwards on a time-scale comparable to protoplanetary disc lifetimes. Systems of larger mass planets such as HD 60532 attain 3:1 resonance as observed. For a given mass accretion rate, results are insensitive to the disc model for the range of viscosity prescriptions adopted, there being good agreement between 2D and 3D simulations. However, in a higher mass disc a pair of Jovian mass planets passes through 2:1 resonance before attaining a temporary phase lasting a few thousand orbits in an unstable 5:3 resonance prior to undergoing a scattering. Thus, finding systems in this commensurability is unlikely.

Key words: accretion, accretion discs – hydrodynamics – methods: numerical – planet–disc interactions – protoplanetary discs – planetary systems.

1 INTRODUCTION

Pairs of extrasolar giant planets in a mean motion commensurability are a common occurrence. It has been estimated that sixth of multi-planet systems detected by the radial velocity technique are in or close to a 2:1 commensurability (Wright et al. 2011). Parameters for some cases of interest that are considered in this paper are shown in Table 1 (for additional examples see e.g. Emelyanenko 2012). In addition, there are two known systems in 3:2 resonance (Correia et al. 2009; Rein et al. 2012; Robertson et al. 2012b) and one in a 4:3 resonance (Johnson et al. 2011; Rein et al. 2012) consistent with the systems in 2:1 resonance being the most commonly observed commensurability.

The existence of these resonant systems indicates that dissipative mechanisms that result in changes to planet semi-major axes that produce related changes to period ratios in planetary systems have operated. This is because the probability of forming resonant configurations *in situ* is expected to be small (e.g. Beauge, Ferraz-Mello & Michtchenko 2012).

Disc–planet interaction can produce the required evolution of the semi-major axes. This may result in convergent migration leading to the formation of a commensurability (see Baruteau et al. 2014 and references therein). Accordingly, understanding the observed configuration of such systems has the potential for either revealing how disc–planet interactions may have operated or for ruling them out.

Previous numerical studies of commensurabilities forming and evolving as a result of disc–planet interactions have focused on systems such as GJ 876, HD 45364 and HD 6805 interacting with disc modelled with either constant kinematic viscosity or with the α-viscosity parameter of Shakura & Sunyaev (1973) taken to be constant (for a review see Baruteau et al. 2014 and references therein). In this paper, we extend such studies, considering systems with orbital parameters similar to those of HD 155358 (Robertson et al. 2012a), 24 Sextantis (Johnson et al. 2011), HD 60532 (Laskar & Correia 2009) as well as HD 6805 (Trifonov et al. 2014) each of which have the inner planet with semi-major axis in the range

★ E-mail: qa208@cam.ac.uk

Table 1. Properties of the HD 155358, 24 Sextantis, HD 6805 and HD 60532 systems. The first three either are or possibly in 2:1 resonance while the fourth is in a 3:1 resonance. The first column identifies the system, and the second column gives the mass of the central star in solar masses. The third and fourth columns give the masses of the planets in Jupiter masses and the fifth and sixth columns give their semi-major axes in au.

System	M_*	M_1	M_2	a_1	a_2
HD 155358	0.92	0.85 ± 0.05	0.82 ± 0.07	0.64	1.02
24 Sextantis	1.54	1.99 ± 0.4	0.86 ± 0.4	1.33	2.08
HD 6805	1.7	2.5 ± 0.2	3.3 ± 0.2	1.27	1.93
HD 60532	1.44	3.15	7.46	0.77	1.58

0.5–1.4 au. We perform 2D and 3D numerical simulations of pairs of giant planets interacting with a protoplanetary disc that attain a mean motion commensurability for up to 2.5×10^4 orbital periods of the inner planet. We investigate whether such systems could have originated at larger radii beyond the ice line and then migrated inwards, the commensurability possibly being formed in the same neighbourhood.

In order to study the role of the nature of the underlying disc model, we consider models with an inner magnetorotational instability (MRI) active region producing a significant effective viscosity and an outer inactive region for which a significant effective viscosity may occur only in the upper layers of the disc (Gammie 1996) as well as models with a uniform α-viscosity prescription throughout. We also consider models with different surface density scaling corresponding to varying the total disc mass or equivalently the steady-state accretion rate. In this way, the disc–planet interaction at different stages of the life of the protoplanetary disc can be studied with lower mass discs corresponding to later stages (e.g. Calvet et al. 2004).

We find that when low-mass disc models are considered, systems with planets in the Jovian mass range maintain a 2:1 commensurability while undergoing inward type II migration. This is found to be at a rate such that formation at a few au from the central star and migration to their current locations on a time-scale comparable to the expected protoplanetary disc lifetime is possible in principle.

We find that there is a relative insensitivity of results to the disc model employed and find good agreement between 2D and 3D simulations. Planets containing larger masses such as the HD 60532 system which is observed to be in 3:1 resonance (Laskar & Correia 2009) are found to attain this resonance in low-mass low-viscosity discs.

We find that for systems with planets in the Jovian mass range, increasing the disc mass results in the formation of an unstable 5:3 resonance. This instability results in the rapid destruction of the commensurability implying that the occurrence of such systems should be less common.

The plan of this paper is as follows. We give the basic equations and coordinate system used in Section 2. In Section 3, we outline the numerical methods and computational domains adopted going on to describe aspects of the physical set-up and disc models used in Sections 3.1 and 3.1.1. We then indicate how results might be scaled to different radii and summarize important aspects of type II migration in Sections 3.2 and 3.3. We go on to describe our numerical results in Section 4, beginning with a comparison with previous results for two migrating planets presented in section 4.1. Finally, we discuss our conclusions in Section 5.

2 BASIC EQUATIONS

We adopt a spherical coordinate system (r, θ, φ) with associated unit vectors $(\hat{\boldsymbol{r}}, \hat{\boldsymbol{\theta}}, \hat{\boldsymbol{\varphi}})$ and origin at the centre of mass of the central star.

The basic equations governing the disc express the conservation of mass and momentum under the gravitational potential due to the central star and any planets and incorporate a kinematic viscosity ν,

$$\frac{\partial \rho}{\partial t} = -\nabla \cdot (\rho \boldsymbol{v}), \tag{1}$$

$$\rho \frac{D\boldsymbol{v}}{Dt} = -\rho \nabla \Phi - \nabla P + \nabla \cdot \boldsymbol{T}. \tag{2}$$

Here the convective derivative is defined through

$$\frac{D}{Dt} \equiv \frac{\partial}{\partial t} + \boldsymbol{v} \cdot \nabla, \tag{3}$$

ρ is the density, $\boldsymbol{v}$ is the velocity, P is the pressure, $\boldsymbol{T}$ is the viscous stress tensor (see e.g. Mihalas & Weibel Mihalas 1984), and Φ is the gravitational potential which has contributions from the central star and any planets present. Disc self-gravity is neglected. The pressure is related to the gas density and the isothermal speed of sound c_s through $P = \rho c_s^2$.

3 NUMERICAL SIMULATIONS

Simulations were performed using the finite volume fluid dynamics code PLUTO (Mignone et al. 2007) which has been used successfully to simulate protoplanetary discs interacting with planets (e.g. Mignone et al. 2012; Uribe, Klahr & Henning 2013). The planet positions are advanced using a fourth-order Runge–Kutta method which however assumes that the forces due to the disc do not change as the planet locations are advanced through a time step, making the method one of lower order (see e.g. Nelson et al. 2000 for comparison). For some runs, we employed the FARGO algorithm of Masset (2000) as this allows the numerical calculations to run significantly faster. We note that for our simulations the options were chosen such that algorithm was applied using the residual azimuthal velocity with respect to the initial azimuthal velocity, the latter not being updated. A sample of runs were checked carefully to confirm numerical stability and that consistent results were obtained (see also Mignone et al. 2012 for a comparison of this type).

For the calculations reported here, we adopt a locally isothermal equation of state for which $c_s \propto r^{-1/2}$. The constant of proportionality is chosen so as to give a constant aspect ratio $h \equiv H/r = c_s/(r\Omega_K) = 0.05$. Here H is the disc semi-thickness and Ω_K is the local Keplerian circular orbit angular velocity. We adopt a system of dimensionless units such that masses are expressed in units of the central stellar mass M_*, radii are expressed in units of the initial orbital radius of the innermost planet and times are expressed in units of the orbital period of a circular orbit at that radius.

For three-dimensional simulations, the radial computational domain in most cases was given in dimensionless units by $r \in [0.15, 3.75]$. The grid outer boundary is treated as a rigid boundary and taken sufficiently far from the planets so that the density perturbations they create in the disc are damped before they reach it, while the grid inner boundary only allows inflow, so that the disc material can be accreted on to the central star. The θ domain was taken to be $[\pi/2 - 3H/r, \pi/2] \equiv [\theta_{\min}, \pi/2]$, with symmetry being assumed

with respect to the plane $\theta = \pi/2$, this being treated as a rigid boundary. The φ domain was taken to be $[0, 2\pi]$.

The standard grid resolution for most simulations was taken to be $(N_r, N_\theta, N_\varphi) = (162, 18, 314)$. The radial grid spacing was non-uniform and chosen so that the grid spacing Δr was equal to $0.02\,r$. This geometric spacing is the most natural one, since the disc semi-thickness scales as r. The azimuthal grid spacing was uniform and such that $\Delta\varphi = \Delta r/r = 0.02$. We remark that disc–planet interactions adopting similar resolutions to those adopted here have been carried out for lower mass planets by Kley, Bitsch & Klahr (2009). The interval $\Delta\theta$ was chosen such that there were six grid cells per scaleheight. Planet gravitational potentials were softened by adopting a gravitational softening length taken to be 0.5 Hill radii, being slightly less than two radial grid cells in extent, and the smoothing filter of Crida et al. (2009a) was employed when calculating torques acting on planets. We also performed convergence checks using simulations for which N_r was increased to 229, N_θ increased to 25 and N_φ was increased to 444, with the softening length reduced by a factor of $\sqrt{2}$.

For two-dimensional simulations, in most cases the radial and azimuthal grids and domains are the same as in the three-dimensional case but now θ is fixed to be $\pi/2$. In this case, the mass density ρ is replaced by the surface density Σ and the pressure is replaced by a vertically integrated pressure. The gravitational softening length was taken to be $0.6H$ and the smoothing filter of Crida et al. (2009a) was employed when calculating torques acting on planets for this case also. The convergence of two-dimensional simulations was checked by performing them at twice the resolution with the softening procedure remaining fixed.

As we consider either low-viscosity discs or discs undergoing steady-state accretion at very low accretion rates, we neglect accretion on to the planet. Many of our runs are carried out with planets migrating in discs with local kinematic viscosity $\nu < 10^{-6}$ in dimensionless units. Accretion on to the planet has been found to be a small effect in this case (Bryden et al. 1999; Kley 1999). In addition, the time required for the accretion rate through the disc to double the planet's mass is significantly longer than the migration time when larger viscosities are considered (see below).

3.1 Disc model and viscosity prescription

For global simulations that need to be run for long times such as those we perform, constraints on numerical resolution are such that small-scale turbulence associated with angular momentum transport has to be modelled through an effective viscosity prescription. To do this, we adopt an α-viscosity prescription (Shakura & Sunyaev 1973). For this, the kinematic viscosity $\nu = \alpha c_s H$. The value of α to be adopted depends on the expected level of turbulence and this in turn depends on the operation of the MRI (Balbus & Hawley 1991). It is expected that there will be an inner MRI active zone together with an outer dead zone which may have active surface layers (Gammie 1996). Small-scale hydrodynamic instabilities such as the vertical shear instability may also contribute in the absence of the MRI (Nelson, Gressel & Umurhan 2013). The location of the interface between these regions depends on details of the transition from magnetohydrodynamic stability to instability and is subject to some degree of uncertainty. Latter & Balbus (2012) estimate that it typically occurs at around 0.6 au. This is illustrated in Fig. 1.

We specify the standard disc model to be such that when the unit of length used to scale our dimensionless units is 1 au and the unit of mass is a solar mass, it corresponds to a steady-state model with accretion rate $\dot{M} = 6.0 \times 10^{-10}\,\mathrm{M}_\odot\,\mathrm{yr}^{-1}$. This is near the bottom of the range of accretion rates observed for protoplanetary discs (Calvet et al. 2004) and might be expected to occur during their late stages which are the focus of attention here. However, we have also considered disc models with surface density scaled such that they are up to 10 times more massive and accordingly with a steady-state accretion rate that is also up to 10 times higher.

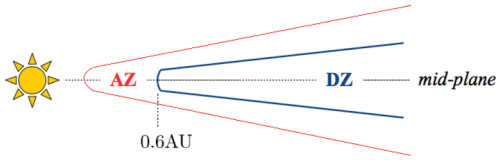

Figure 1. Illustration of our disc model, which contains an inner MRI active zone (AZ) together with an outer disc with reduced activity. This may have a dead zone (DZ) together with an active surface layer. The transition radius between those two regions is located at 0.6 au. For standard runs, α does not vary with θ or height in the disc. The value of α then decreases sharply from $\alpha_{\rm AZ} = 10^{-3}$ to $\alpha_{\rm DZ} = 10^{-4}$ as the transition radius is passed through. For the layered model, α is only non-zero for $[\pi/2 - 3H/r, \pi/2] \equiv [\theta_{\rm min}, \pi/2]$ in the outer disc.

To allow for an inner MRI active region together with an outer region with much less activity, we specify α to be a function of r. Thus $\nu = \alpha c_s H$, where

$$\alpha = \alpha_{\rm DZ} + \frac{\alpha_{\rm AZ} - \alpha_{\rm DZ}}{1 + \exp\left(-25\left(1 - \dfrac{r}{0.6}\right)\right)}. \quad (4)$$

Here $\alpha_{\rm AZ}$ corresponds to the inner region and $\alpha_{\rm DZ}$ corresponds to the outer zone. Our standard model has $\alpha_{\rm AZ} = 10^{-3}$ and $\alpha_{\rm DZ} = 10^{-4}$. The functional form of α gives a sharp transition around $r = 0.6$. The surface density is chosen to provide the prescribed accretion rate through the relation $\dot{M} = 3\pi\nu\Sigma$. This gives $\Sigma \propto r^{-1/2}$ when α is constant.

3.1.1 *Layered model*

In order to consider the possibility that a significant effective disc viscosity arises only in the upper layers of the outer disc (e.g. Gammie 1996), we have performed simulations for a layered outer disc model. In this model, α was taken to be non-zero only in the upper half of the θ domain, namely $[\theta_{\rm min}, (\theta_{\rm min} + \pi/2)/2]$ (see Fig. 1). The value of α in the upper domain was chosen to be such that the integrated stress in the meridional direction was the same as for an outer disc model with α independent of θ (see Pierens & Nelson 2010). In practice, the value of α in the upper layers of the layered model was thus found to be 7.5 times larger than the value for the corresponding non-layered model.

For three-dimensional models, the disc equilibrium pressure is given by

$$P = P_0(R)\exp\left(\frac{GM_*}{c_s^2 r}\ln(\sin\theta)\right). \quad (5)$$

Here $R = r\sin\theta$ and the function P_0 can be chosen to match a prescribed surface density or alternatively mid-plane pressure or density.

3.1.2 *Initial gaps*

In the simulations presented here, the density or surface density was modified such that any planets were initially placed within gaps. The initial orbital evolution would differ if the planets were

initially embedded. However, because our goal is to measure steady-state migration rates, this is not a problem. Thus, the simulations are assumed to commence after any gaps have been formed. In this way, we avoid having to simulate an uncertain initial phase during which gaps are formed.

The procedure we adopted was to reduce the density or surface density by a constant factor in the interval $[r_p/1.15, 1.15r_p]$ where r_p is the initial orbital radius of the planet, being assumed to be in a circular orbit. This profile was then joined to the original through linear connections in the intervals $[0.9r_p/1.15, r_p/1.15]$ and $[1.15r_p, 1.265r_p]$. The gap reduction factor was taken to be a factor of 10 in most cases, being a factor of 100 for the cases with planets with final masses exceeding 2 Jupiter masses.

In addition, the planets were held in fixed circular orbits for 200 orbits before being released. Their masses were built up to their final values over the first 20 orbits using the procedure given by de Val-Borro et al. (2007).

3.2 Scaling to arbitrary radii

The results obtained with the unit of radius chosen to be the initial orbital radius of the inner planet can be scaled to apply to arbitrary radii. This is done by noting that results are invariant if the length-scale is multiplied by λ, the time-scale is multiplied by $\lambda^{3/2}$ and the mass scale left unaltered. To be consistent with this, the surface density should be reduced by a factor λ^2. If regions of the disc are connected in this way, the situation does not correspond to a steady-state disc. However, this is not unreasonable if it is applied at radii where the age or evolution time of the system is less than the local viscous time-scale. For our standard disc model, this would be the case for length-scale exceeding 2 au and age $\lesssim 2 \times 10^6$ yr.

We note that when applied, the scaling procedure shifts the transition radius between the active and inactive regions while its location should in principle remain constant. However, this is not a problem as we find an insensitivity of our results to the location of the transition radius as long as the planets migrate in the outer disc (see below).

3.3 Aspects of type II migration

The planets in the simulations presented here are massive enough to make deep gaps in the disc surface density profile. Accordingly, they undergo type II migration (e.g. Lin & Papaloizou 1986, Lin & Papaloizou 1993; Baruteau et al. 2014). The rate of migration is governed by the viscous time-scale and the disc mass within a radial scale comparable to its orbital radius, r. Baruteau et al. (2014) estimate the migration rate of a planet of mass M_i as τ_m^{-1}, where

$$\tau_m = \tau_\nu \max\left(1, \frac{M_i}{4\pi\Sigma r^2}\right), \quad (6)$$

with τ_ν being a viscous time-scale. Thus, when the planet mass becomes large, the evolution rate slows on account of the inertia of the planet. Note that Ivanov, Papaloizou & Polnarev (1999) obtain a faster rate than implied by equation (6), finding that the second term in the parentheses appears taken to a fractional power. The rate is faster because disc material tends to pile up near the outer gap edge increasing the angular momentum flux that the planet needs to provide in order to maintain it.

4 NUMERICAL RESULTS

4.1 Comparison with previous results

Because our simulations of planet–disc interaction with the PLUTO code were implemented from scratch, we begin by establishing that some of the main results obtained in previous studies are recovered with our code. In particular, we focus on the much studied GJ 876 system (see e.g. Snellgrove, Papaloizou & Nelson 2001; Kley et al. 2005; Crida, Sándor & Kley 2008), as well as a case involving the action of the so-called Masset–Snellgrove mechanism invoked to reverse type II migration (Masset & Snellgrove 2001) that has been considered by Crida, Masset & Morbidelli (2009b).

4.1.1 The case of GJ 876

Our first comparison run was initiated with the mass ratio equal to 6×10^{-3} for the inner planet, and 1.8×10^{-3} for the outer planet. These parameters correspond to those of GJ 876. The simulation employed the physical set-up described in Snellgrove et al. (2001, see their section 3.1). A constant aspect ratio $h = 0.07$ and a constant α-viscosity prescription with $\alpha = 2 \times 10^{-3}$ are adopted. The two planets are initially in circular orbits, and start their evolution with semi-major axis $a_1 = 1.0$ for the outer planet and $a_2 = 0.6$ for the inner planet. Note that for this comparison, we adopt their nomenclature and system of dimensionless units. Hence, the outer planet is initially located outside the exact 2:1 commensurability ($a_1 \sim 0.95$).

A putative uniform initial disc surface density Σ_0 corresponding to what would give a disc mass of $2M_J$ within the initial orbit of the outer planet was taken. It is also assumed that both planets are located inside a tidally truncated cavity located at $r < 1.3$, with low surface density equal to $0.01\Sigma_0$. In the region $1.3 < r < 1.5$, the surface density is prescribed such that $\ln\Sigma$ linearly joins to $\ln\Sigma_0$. In addition in our run, the smoothing filter of Crida et al. (2009a) was used when calculating torques acting on planets.

The results are displayed in Fig. 2 which can be compared with fig. 1 of Snellgrove et al. (2001). The two planets first undergo a phase of convergent migration. At time $t \sim 400$ orbits, the period ratio between the two planets locks around the value 2, and the resonant angle $2\lambda_2 - \lambda_1 - \varpi_1$ starts to librate around 0. Here λ_2, λ_1, ϖ_2 and ϖ_1 are the longitudes of the inner and outer planet and the longitudes of pericentre for the inner and outer planets, respectively. A 2:1 mean motion resonance is subsequently maintained. The behaviour we obtain is very similar to that found by Snellgrove et al. (2001) until a run time 1500 orbits is reached. After this, the evolution of the semi-major axes and eccentricities stall in their run while they continue to respectively decrease and increase slightly in ours. We believe that the stalling is artificial and due to the approach of the inner planet to the inner boundary, located at a radius equal to 0.4 in their case. In order to avoid this, we chose an inner boundary radius $r_{in} = 0.2$. This allowed us to continue the evolution of the two planets for up to 3000 orbits without this type of influence from the inner boundary. In the context of the above discussion, we remark that Kley et al. (2005) performed simulations with the inner planet totally interior to the calculation domain. They found that its eccentricity continued to increase as we did (see their fig. 10).

4.1.2 An example illustrating the Masset–Snellgrove mechanism

Masset & Snellgrove (2001) found that the migration of two planets locked in a mean motion resonance can proceed outwards. For this

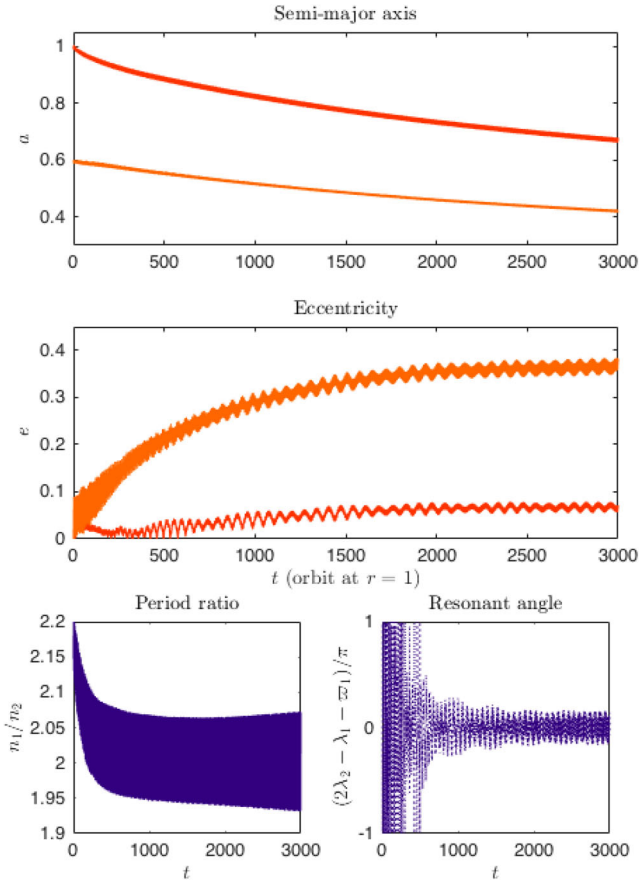

Figure 2. Results from the GJ 876 comparison run. The uppermost panel shows the evolution of the semi-major axes of the two planets, the middle panel shows the eccentricities (the upper curve corresponding to the inner planet), the left-hand bottom panel shows the period ratio for the two planets and the right-hand bottom panel shows the resonant angle $2\lambda_2 - \lambda_1 - \varpi_1$. The unit of time, t, in this and subsequent figures is the orbital period at a value of the dimensionless radius equal to unity.

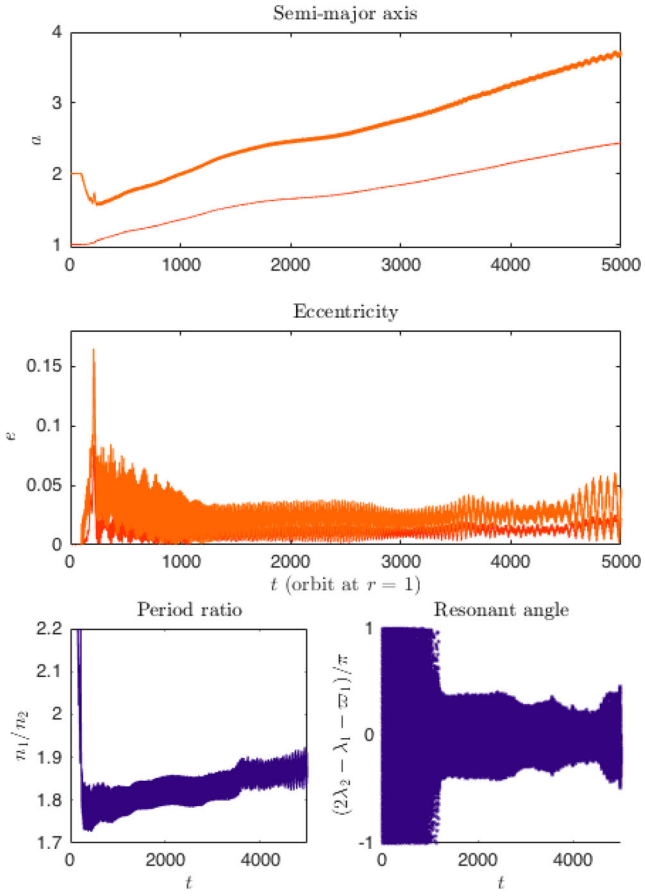

Figure 3. Results from the run illustrating the Masset–Snellgrove mechanism. The panels correspond to those of Fig. 2.

to occur, they must open overlapping gaps and the outer planet be of significantly lower mass than the inner one. Our second comparison run was chosen such that this mechanism is expected to operate. It was initiated with mass ratios for the inner and outer planets respectively equal to 3×10^{-3} and 10^{-3}. These parameters correspond to those adopted by Crida et al. (2009b). The simulation adopted their physical set-up apart from the treatment of the boundaries (see their section 3.2). They employ an additional matched one-dimensional simulation of a putative enveloping disc, whereas we adopt our standard conditions described above. As the inner boundary radius is located at a radius equal to 45 per cent of the initial inner planet orbital radius and the interior disc plays a major role in driving the outward migration, we expect differences in results at early times. The outer boundary may also become significant at late times. The form of the aspect ratio adopted is $h = 0.045 \times (r/a_0)^{1/4}$ (a_0 being the initial inner planet orbital radius), the initial surface density is $\Sigma(r) = \Sigma_0 \times (r/a_0)^{-3/2}$ with $\Sigma_0 = 1.5 \times 10^{-3}$ and an α-viscosity prescription with $\alpha = 0.01$ is adopted. The two planets are held in circular orbits for the first 100 orbits of the inner planet, and start their evolution with semi-major axis $a_1 = 1 = a_0$ for the inner planet and $a_2 = 2$ for the outer planet.

The results are displayed in Fig. 3 which can be compared with fig. 1 of Crida et al. (2009b). After the release, both planets start to migrate inwards. The outer planet moves rapidly in a type III migration regime with the inner one moving much more slowly corresponding to type II migration. This convergent migration of the two planets causes passage through the 2:1 mean motion resonance. The resonant angle $2\lambda_2 - \lambda_1 - \varpi_1$ starts librating around zero from time $t \sim 1000$. Subsequently, the convergent migration stops and the two planets migrate smoothly outwards together.

The qualitative behaviour described above is very similar to that obtained by Crida et al. (2009b). However, they obtain an acceleration at early times followed by a significant slow-down later on, whereas in our case the outward migration rate is more uniform. As indicated above, this difference is not unexpected on account of the role of the inner boundary. Thus, we find that just after the planets start moving outwards, the inner planet initially migrates outwards at half the rate obtained by Crida et al. (2009b). However, after 5000 orbits at $r = a_0$ (corresponding to a time $t \sim 1.12 \times 10^5$ yr in Crida et al. 2009b), when the inner boundary is expected to be less important, the mean migration rates are approximately the same.

4.2 The standard run

We now consider the runs that are the focus of this paper which, unlike in Section 4.1.2, involve for the most part inward convergent migration of the planets. For these cases as well as that of GJ 876, an overview can be obtained by considering a simple N-body model in which the planets move as particles under their gravitational interaction and the influence of additional forces presumed to arise from interacting with the disc (see e.g. Snellgrove et al. 2001;

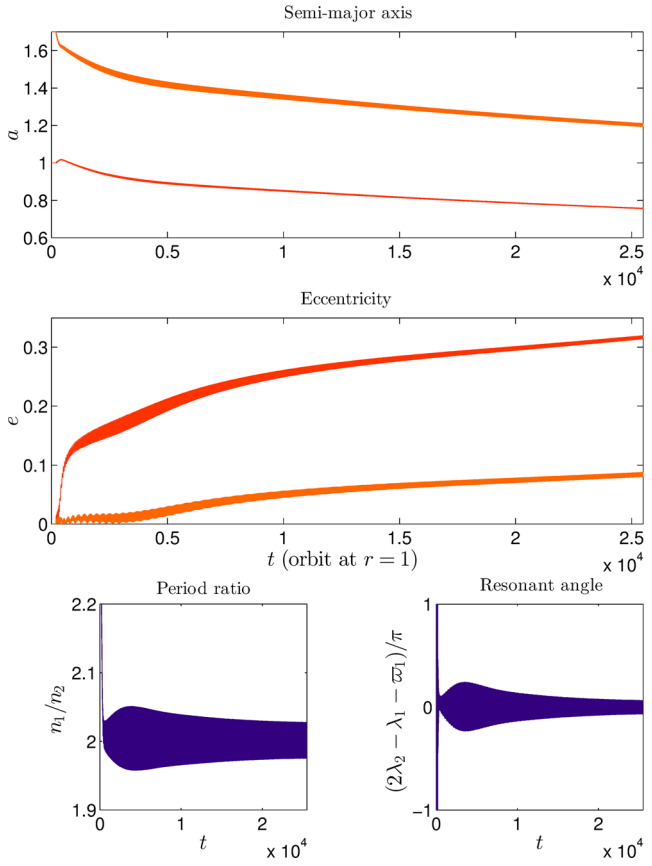

Figure 4. Results for the 2D standard run. The panels correspond to those of Fig. 2.

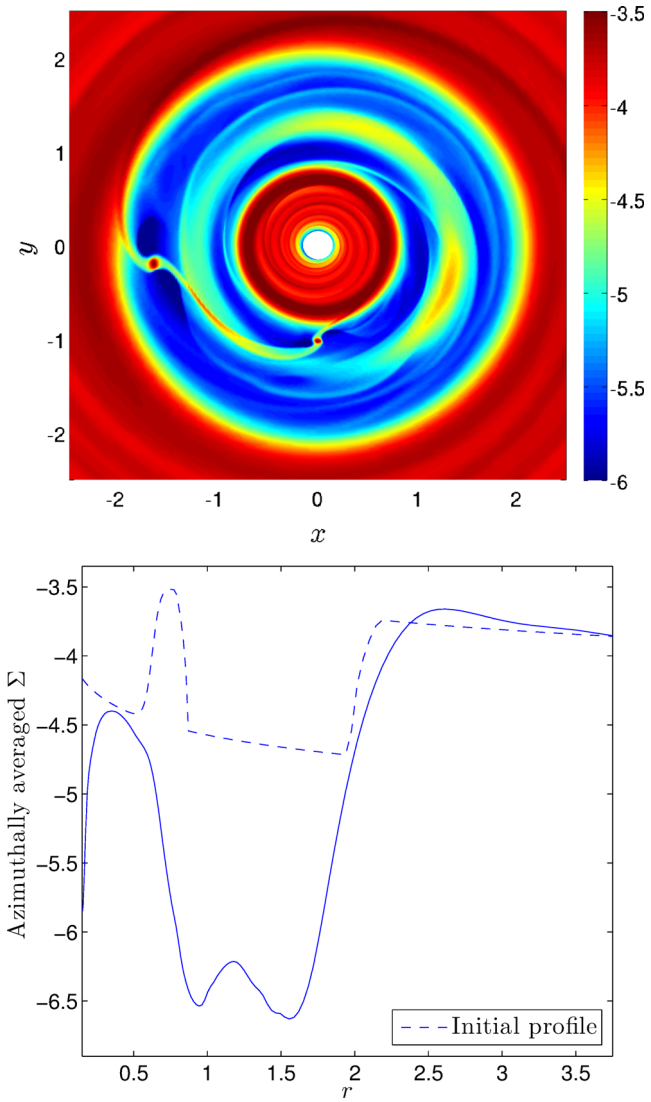

Figure 5. The upper panel shows surface density contours in logarithmic scale for the disc after 280 orbits of the simulation shown in Fig. 4. The lower panel shows the azimuthally averaged surface density in logarithmic scale after 3750 orbits (solid curve) and the initial surface density (dashed curve). The planets occupy the deep common gap.

Lee & Peale 2002; Nelson & Papaloizou 2002). These result in orbital circularization and migration. It is found that unless the convergent migration is very rapid, the planets attain a commensurability and then migrate together maintaining it. As they do so, their eccentricities increase until either their migration halts or their rate of growth can be balanced by a damping process.

For the slowest migration rates, a 2:1 resonance is attained for Jovian mass planets while for larger masses a 3:1 resonance can be attained. As the rate of convergence is increased, closer commensurabilities are attained. Our results are fully in line with these general expectations. The rate of convergent migration and hence the closeness of the commensurability is determined by the rate of angular momentum transport in the disc which for a fixed α distribution increases with the mass in the disc.

The 2D standard run was initiated with the mass ratio for both planets equal to 10^{-3}. Noting that they are somewhat uncertain, these parameters may approximately correspond to those for HD 155358 and 24 Sextantis (see Table 1). The simulation was initiated with the planets occupying a common gap in the standard disc as described above. We assume that they start their evolution with semi-major axis $a_1 = 1$ for the innermost planet and $a_2 = 1.7$ for the outermost planet in dimensionless units. The results are plotted in Fig. 4. The evolution of the semi-major axes and eccentricities are shown for a time interval of 2.5×10^4 time units. The system enters 2:1 resonance after a few hundred orbits. Note that in this and other cases, the inner planet migrates outwards at early times on account of the influence of the inner disc. The lowermost left-hand panel shows the evolution of the orbital period ratio n_1/n_2 of the two planets, n_1 and n_2 denoting the mean motions of the inner and outer planet, respectively. An ultimate libration amplitude of a few per cent is indicated. The lowermost right-hand panel of Fig. 4 shows the resonance angle, $2\lambda_2 - \lambda_1 - \varpi_1$, appropriate for the 2:1 resonance. This resonance angle ultimately librates around zero. The behaviour of the second resonance angle, $2\lambda_2 - \lambda_1 - \varpi_2$, is very similar.

At late times, the migration time $-r/\dot{r} \sim 1.5 \times 10^5$ inner planet initial orbital periods. For comparison, the viscous time $2r^2/(3\nu)$ for the outer disc is 4.2×10^5 orbits at $r = 1$ in dimensionless units. Note that the two resonantly coupled planets migrate at a similar rate as a single planet (see below).

Additional results from the 2D standard run are illustrated in Fig. 5. The upper panel shows surface density contours for the disc after 280 orbits and the lower panel shows the azimuthally averaged surface density gap after 3750 orbits. Note the non-axisymmetric vortex-like structures in the low surface density ring between the planets (see e.g. de Val-Borro et al. 2007). The planets occupy a

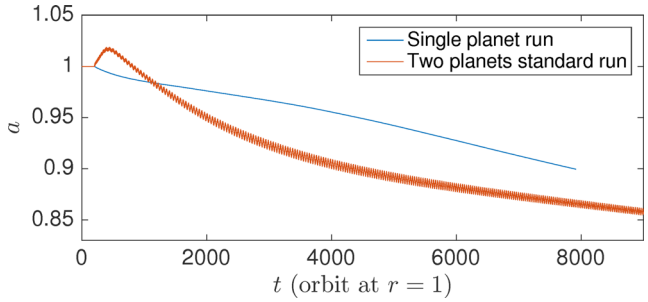

Figure 6. Evolution of the semi-major axis of a single planet with mass ratio 10^{-3} migrating in a standard disc plotted together with the evolution of the semi-major axis for the innermost planet in the standard run. The evolution is shown as a function of time expressed in units of the orbital period at $r = 1$ in dimensionless units.

deep common gap that is characteristic of the simulations reported here.

In Fig. 6, we illustrate the migration of a single planet in a standard disc. For comparison, the evolution is plotted together with that for the inner planet in the standard case. At the beginning, the evolution in the standard case is outwards. This is because the planet starts in a much wider gap and is pushed outwards by the inner disc in that case. However, once the system attains resonance, the planet is pushed inwards by the inwardly migrating outer planet. For the isolated planet, the inward migration is driven by the outer disc directly. In both cases, we expect a characteristic migration rate corresponding to type II migration and indeed the rates are found to be ultimately comparable. The migration speed of the single migrating planet attains a steady value between 5000 and 8000 orbits. The mean migration time-scale over this period is estimated as $\langle -r/\dot{r}\rangle \sim 6.9 \times 10^4$ orbits at a dimensionless radius of unity. This is characteristic of type II migration, an aspect that is discussed further in Section 5.

4.2.1 *An entirely active disc*

Fig. 7 shows results for a simulation with the same conditions, including the initial set-up of the pair of planets, as for the 2D standard run, except that only an active model disc was used. That is the transition radius of $r = 0.6$ for the standard run was effectively moved to very large radii. The quantities plotted in the various panels of Fig. 7 correspond to those plotted in the corresponding panels of Fig. 4 and the results are qualitatively very similar. The estimated late-time migration time $-r/\dot{r} \sim 2.4 \times 10^5$ orbits is significantly shorter than in both the standard two-planet case and the single-planet case where the planet migrates in the inactive region. This is because even though the viscosity is 10 times larger in the active disc, the surface density is 10 times smaller resulting in a slower migration rate on account of the reduced disc mass in the neighbourhood of the planets.

4.2.2 *A disc without an inner active region*

In Fig. 8, we illustrate a 2D two-planet run with the same parameters as the standard run except that the inner active disc was removed or equivalently the transition radius was moved to very small values. The quantities shown in the panels of Fig. 8 are the same as in the corresponding panels of Fig. 4. The migration time-scale at later times is estimated to be $-r/\dot{r} \sim 10^5$ orbits at a dimensionless radius of unity. This is almost exactly the same as for the standard case at

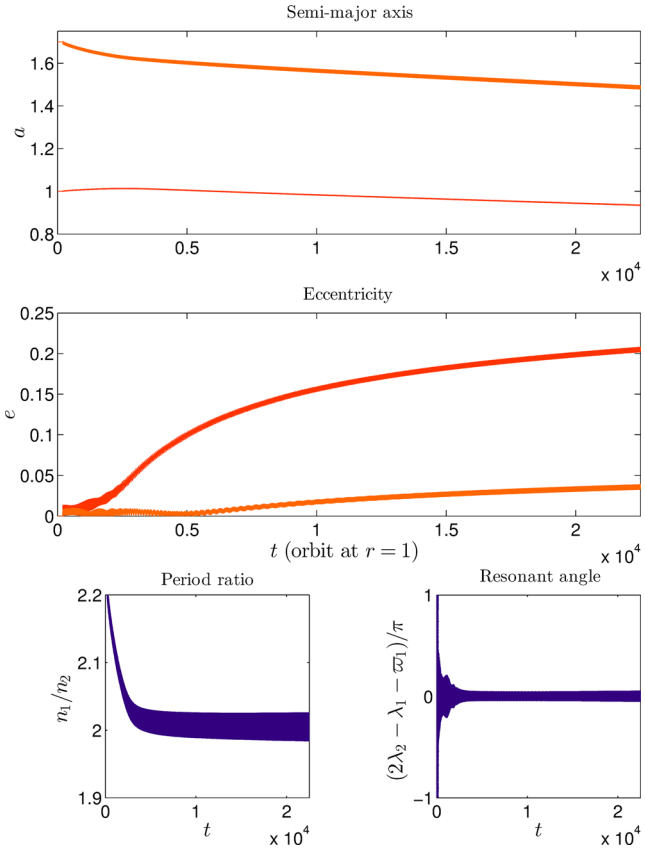

Figure 7. Results of a simulation with the same conditions as for the 2D standard run except that only an active model disc was used. That is the transition radius of $r = 0.6$ for the standard run can be regarded as being moved to a very large value. The panels correspond to those of Fig. 4. Note that the migration is significantly slower than in the standard case.

the same time. Note that the eccentricities at times corresponding to the same amount of relative joint migration are smaller in this case than those for the corresponding standard case, which is indicative of a larger damping rate.

4.2.3 *Three-dimensional simulations*

We now consider 3D simulations. The disc models were set up as described in Sections 3.1 and 3.1.1 with the planets introduced together with initial gaps as described in Section 3.1.2. We recall that for the standard 3D model α does not vary with θ.

A comparison of the evolution of the semi-major axes for the standard 2D two planet with the corresponding results from the standard 3D run is given in the upper panel of Fig. 9. The evolution of the eccentricities is shown in the lower panel. These are found to be in very good agreement with each other and therefore also in accord with the simplified N-body approach mentioned above. This suggests that the evolution can be determined by considering the 2D response of the vertically averaged disc. The fact that the response is for the most part two-dimensional is indicated by the behaviour of the disc state variables. We show density contours in logarithmic scale for three indicated values of θ at a typical late time of 1100 orbits after the start of the simulation in Fig. 10. These values correspond to the mid-plane and approximately to heights H and $2H$ above it. It will be seen that apart from in the neighbourhoods of the planets, the density distributions are approximately the same at the

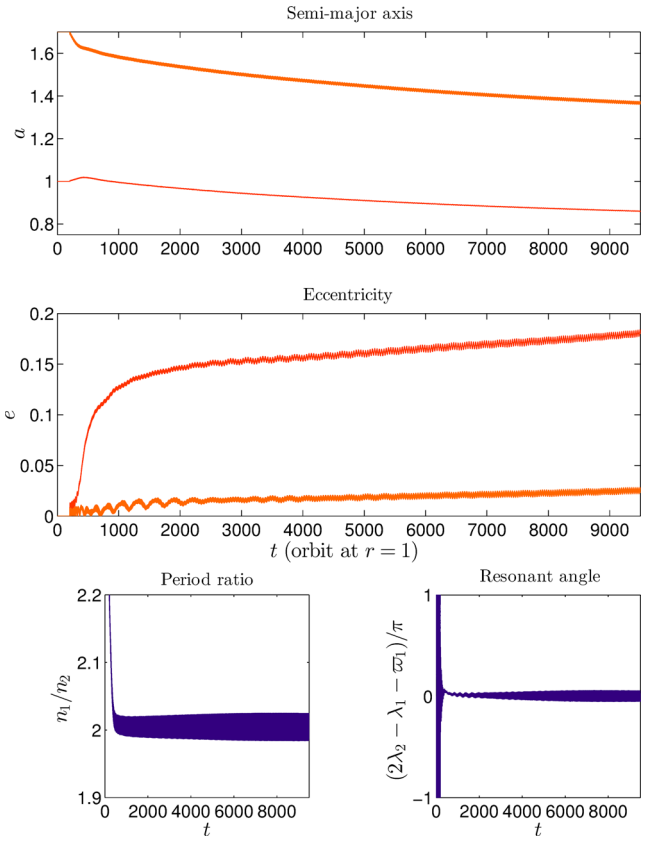

Figure 8. As for the 2D standard run shown in Fig. 4 except that in this case the disc model was such that the inner active disc was removed or equivalently the transition radius can be regarded as being moved to a very small value. The panels correspond to those of Fig. 4.

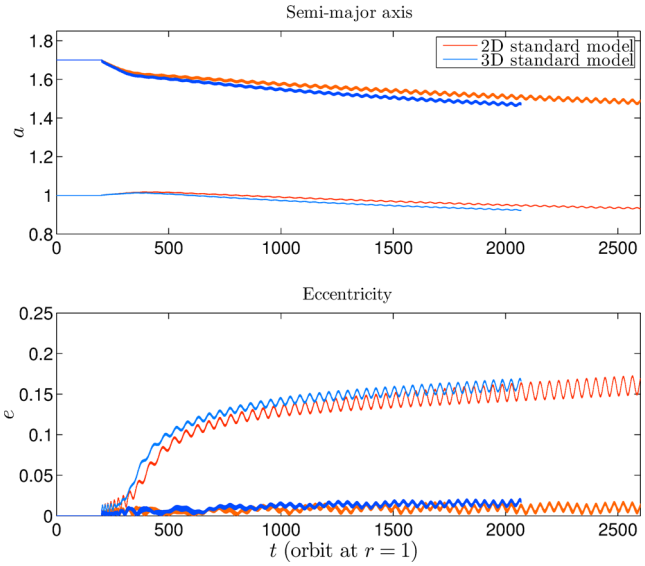

Figure 9. Comparison between the 2D and 3D standard runs. A comparison of the evolution of the semi-major axes is given in the upper panel. The lower panel shows the evolution of the eccentricities with the upper pair of curves corresponding to the inner planet.

different heights apart from a constant scaling factor. In the neighbourhoods of the planets, there are the local mass concentrations usually seen in 2D simulations (see the left-hand panel of Fig. 10). In the upper regions of the disc, these are absent and there is instead material depletion on account of vertical flows towards the planets. To illustrate this aspect, Fig. 11 shows the characteristic form of the stream lines in a meridional section at the azimuth of the inner planet. These are shown after a time corresponding to 1410 orbits at dimensionless radius equal to unity. Significant vertical motions associated with material moving from the upper regions of the disc towards the mid-plane slightly interior to the location of the centre of gravity of the planet are apparent. This is an effect that can only be represented in 3D. However, this is not found to cause significant departures from the 2D results for the orbital evolution, presumably because of the small amount of material in the gap regions near to the planets. We remark that a similar behaviour of the state variables to that described here was found by Pierens & Nelson (2010) in their 3D simulations with a single planet.

4.2.4 *Layered model*

A comparison of the results obtained for the layered model described in Section 3.1.1 with those obtained from the standard 2D model is illustrated in Fig. 12. The layered disc model had the same integrated stress in the meridional direction as in the standard case. Apart from the differing disc model, the conditions are the same as for the standard 3D run. It will be seen that the evolution of the semi-major axes for the two runs is almost identical. We remark that the migration rates for both planets are slightly faster in the standard case as compared to the simulation with the layered model. This is

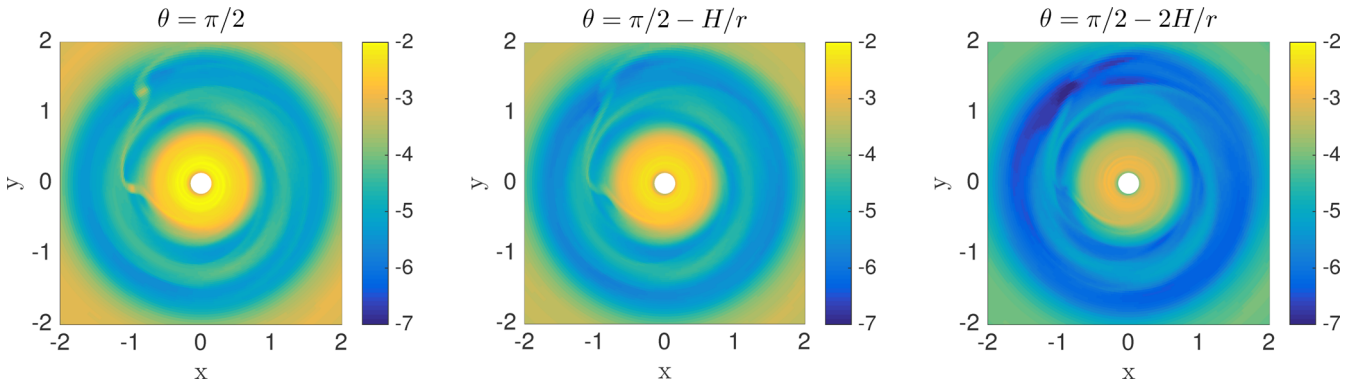

Figure 10. Contours of log ρ in dimensionless units in the (r, φ) plane are shown for three indicated values of θ for the 3D standard run after 1100 orbits. From left to right, these values correspond to the mid-plane and approximately to heights H and $2H$ above the mid-plane.

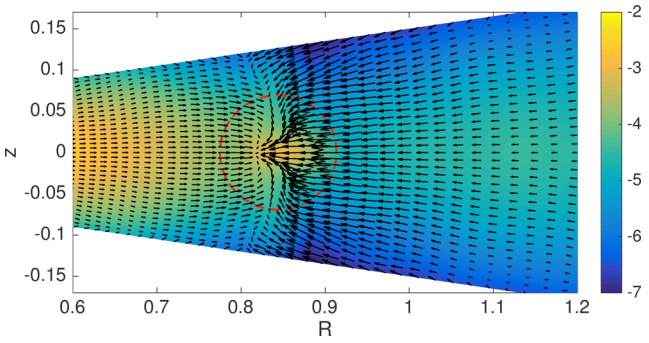

Figure 11. Stream lines in a meridional section at the azimuth of the location of the inner planet for the 3D standard run after 1410 orbits. The colour scale indicates log ρ in dimensionless units and the dashed circle indicates the location of the surface of the Hill sphere.

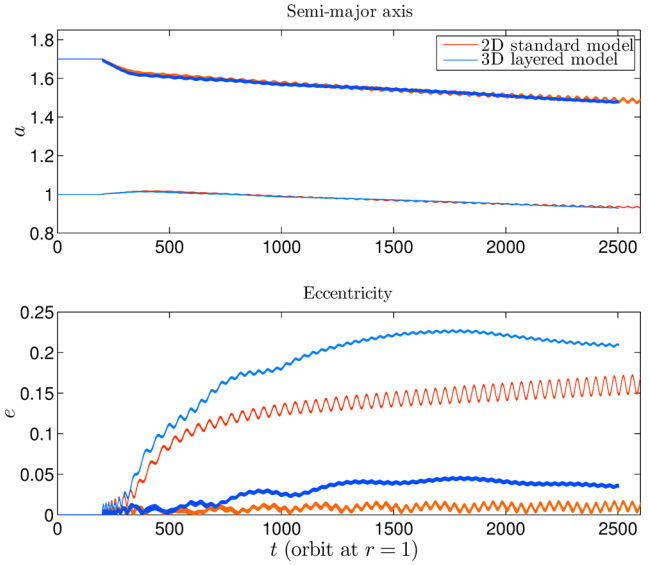

Figure 12. Results for the 3D layered model compared to those of the 2D standard run. The panels correspond to those of Fig. 9. Note that the lower panel shows the evolution of the eccentricities with the uppermost pair of curves corresponding to the inner planet.

in line with the results of Pierens & Nelson (2010) for the case of a single Jupiter mass planet.

However, the eccentricities are significantly larger at corresponding times for the layered model. This indicates that the eccentricity damping rate is lower in this case and accordingly it depends on the detailed properties of the disc model. For the layered model, we recall that the disc is inviscid near the mid-plane.

4.3 Increased disc surface density and the formation of a 5:3 resonance

In order to investigate the effect of increasing the disc surface density, we performed 2D two-planet runs with the same parameters as the standard run, except that the disc model was modified such that the surface density was increased by a factor of 5. From the discussion of the disc models in Section 3.1, this corresponds to increasing the steady-state accretion rate by the same factor.

The results for this case are illustrated in Fig. 13. The uppermost panel shows the semi-major axes, the middle panel the eccentricities, the left lowermost panel shows the period ratio and the right lowermost panel shows a resonant angle.

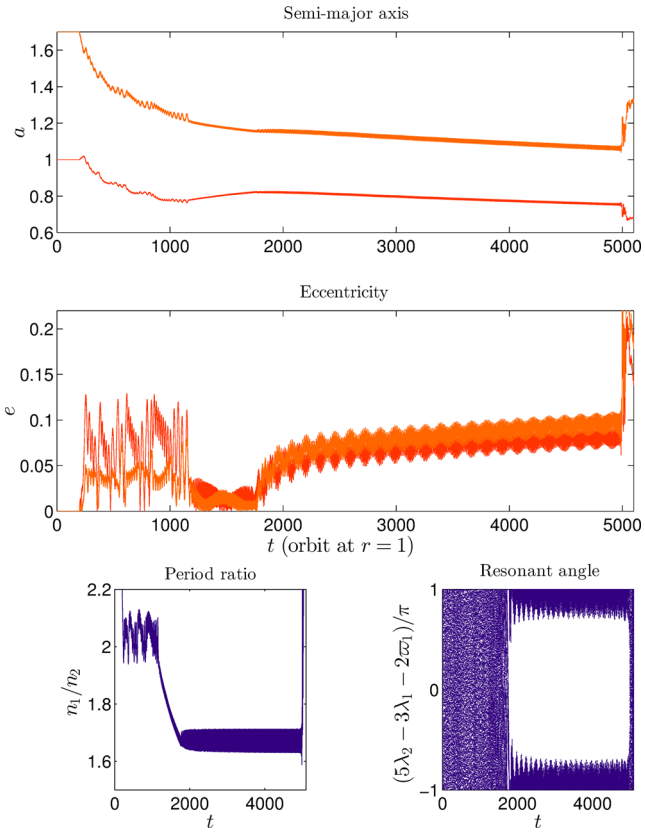

Figure 13. Results for a 2D two planet run with the same parameters as for the standard run, except that the initial disc model was modified such that the surface density was increased everywhere by a factor of 5. The panels correspond to those of Fig. 4, except for the lowermost right-hand panel which shows the resonant angle $5\lambda_2 - 3\lambda_1 - 2\varpi_1$, appropriate for the 5:3 resonance. Note that the middle panel shows the evolution of eccentricities, with that of the inner planet initially mostly smaller but with the curves for the two planets later overlapping. This run eventually goes unstable after approximately 5000 inner planet orbits.

The outer planet initially migrates rapidly in a type III migration regime while the semi-major axis of the inner planet hardly changes, indicating an approximate balance between inward and outward migration torques. As a consequence, the planets rapidly enter a 2:1 resonance which quickly develops an instability, as indicated by the strong fluctuations in eccentricity and period ratio. The instability causes the planets to leave the resonance at around $t = 1000$ and resume convergent migration. During this phase, the inner planet migrates slowly outwards on account of the action of the inner disc and a deeper common gap. The planets enter a 5:3 resonance at $t \sim 2000$. This persists until time $t \sim 5000$. Accordingly, the resonant angle shown is $5\lambda_2 - 3\lambda_1 - 2\varpi_1$. This librates about π once the resonance forms. The angle $5\lambda_2 - 3\lambda_1 - 2\varpi_2$ shows very similar behaviour. Although the estimated inward migration time $-r/\dot{r} \sim$ 50 000 inner planet initial orbital periods, while the system is in 5:3 resonance this run eventually goes unstable after approximately 5000 orbits culminating in the two planets undergoing a scattering (see also Lee, Thommes & Rasio 2009, for an approach based on N-body methods). Thus, observing a system in 5:3 resonance is unlikely. We remark that although the planet mass ratios differed and the transition was from a 2:1 resonance to a 3:2 resonance,

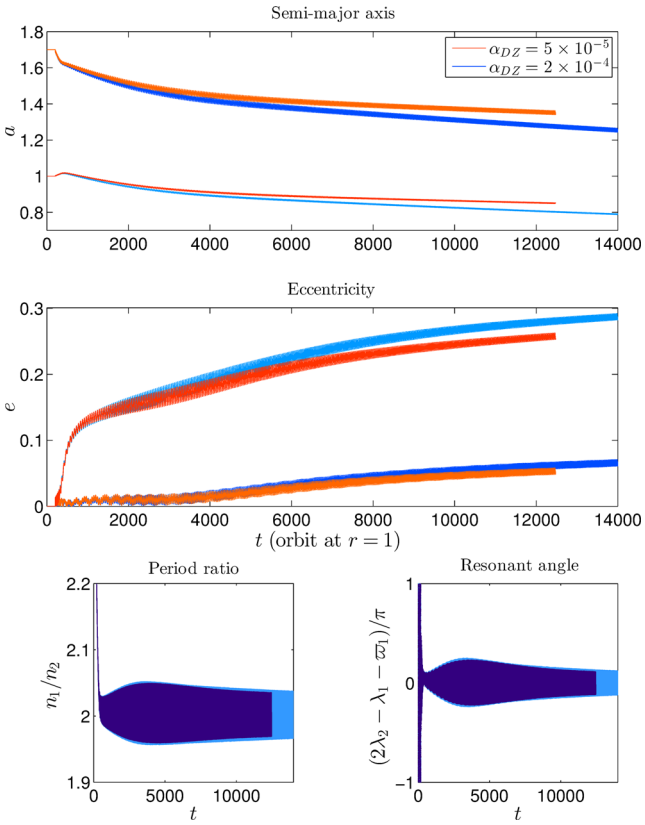

Figure 14. A comparison of two 2D runs which were identical to the standard case except that the values of α in the dead zone were taken to be 2×10^{-4} and 5×10^{-5}, respectively. The panels correspond to those in Fig. 4. The period ratio and resonant angle plots overlap for these cases.

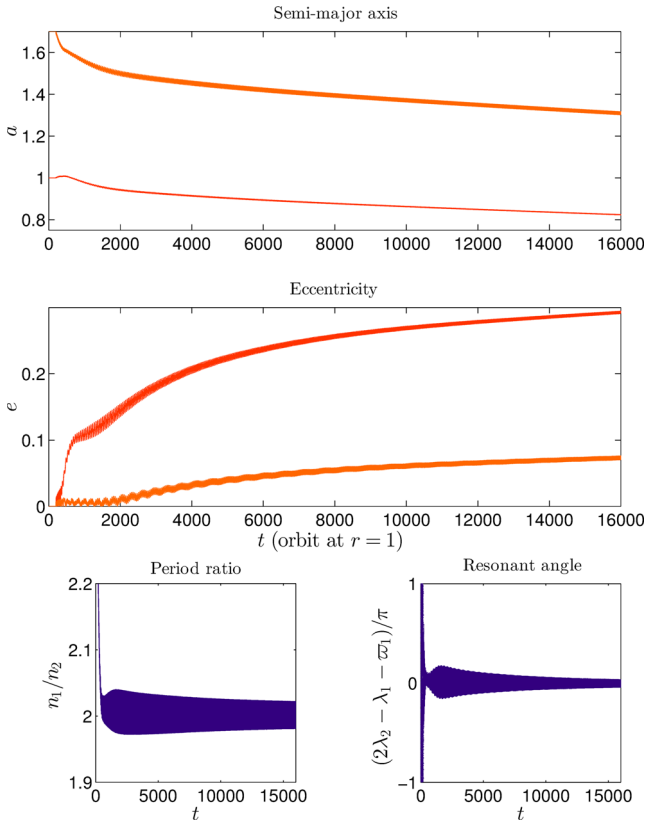

Figure 15. Results for a 2D run which was identical to the standard case except that the value of α in the active zone was taken to be 10^{-2}. The panels correspond to those in Fig. 4.

qualitatively similar behaviour to that described above, up until the instability at late stages, was found in simulations of Rein, Papaloizou & Kley (2010, see their fig. 6).

In order to investigate further the effect of increasing disc mass, we performed an additional simulation for which the disc mass was increased by a factor of 10. In this case, the surface density is large enough that the Toomre criterion for gravitational instability is close to being marginal at the outer boundary, that being potentially the most unstable location. As self-gravity has been neglected, this disc model provides the maximum strength of the disc planet interaction that we can consider. We investigate it in order to check that it is the model for which the closest commensurability is attained as indicated by the discussion at the beginning of Section 4.2.

This case behaves similarly to the previous one except that the initial migration phase is more rapid and such that the system passes straight through the 2:1 resonance before going into an unstable 5:3 resonance. After 2000 orbits, it then undergoes a transition to a stable 3:2 resonance where it remains until 10 000 orbits after the start of simulation. While the system in the 3:2 resonance, the mean migration rate is approximately 50 per cent faster than for the previous case. As expected, the closest commensurability was attained in this case.

4.4 The effect of changing the magnitude of the viscosity

In order to examine the effect of changing the magnitude of the viscosity, a comparison of the semi-major axis evolution for different 2D runs is given in Fig. 14. For these runs, the value of α in the outer inactive region was increased and decreased by a factor of 2 as compared to the standard run, while the surface density was scaled such as to maintain the same steady-state accretion rate as for the standard run. The inner active disc region was the same as in the standard case. The quantities plotted in the different panels are as in Fig. 4. We see that the migration rate decreases with decreasing viscosity as expected but somewhat less steeply than linearly. This is because the migration rate has a dependence on the disc surface density profile which takes a long time to evolve, especially in the case with the smallest viscosity.

In Fig. 15, we present a 2D run for which the initial conditions were as in the standard case except that the value of α in the inner active region was increased from 10^{-3} to 10^{-2}. The quantities plotted in the different panels are as in Fig. 4. The results on this case are very similar to those obtained for the standard run. We remark that the planets are migrating in the inactive part of the disc. Accordingly, this result indicates that the inner active disc plays only a minor role in these circumstances.

4.5 A case with a more massive outer planet

We have also considered the effect of increasing the mass of the outer planet. In Fig. 16, we give the results for a simulation for which the mass ratio of the outer planet was increased by a factor of 2 and its starting distance was increased from 1.7 to 2 in dimensionless units otherwise initial conditions are as in the standard model. However, the surface density was everywhere taken to be 78 per cent of the standard value. This was done so as to make the disc mass in the neighbourhood of the outer planet the same as in the standard case.

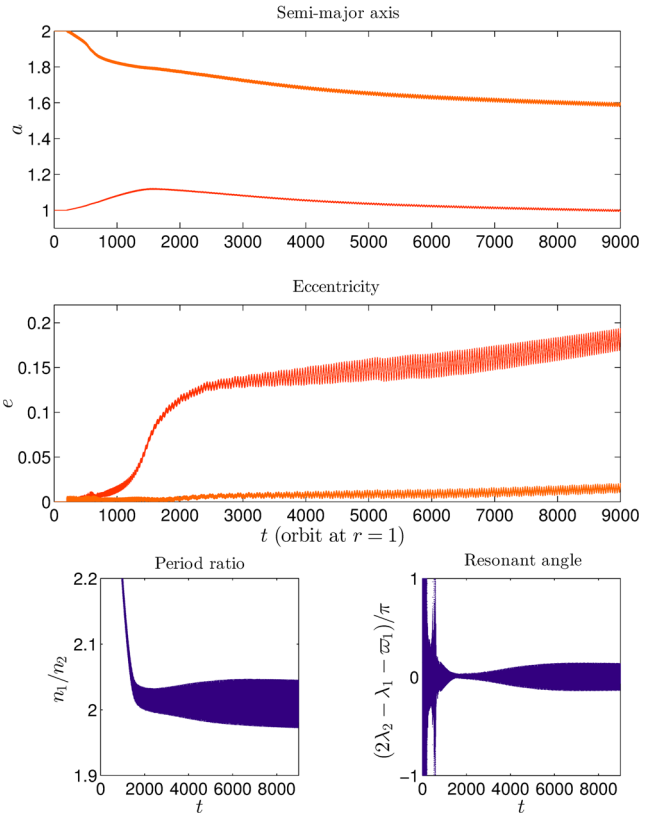

Figure 16. As for the standard case shown in Fig. 4 except that the surface density in the initial disc model is reduced through multiplication by a factor 0.78. In addition, the mass of the outer planet which starts further out at $r = 2$ is increased by a factor of 2.

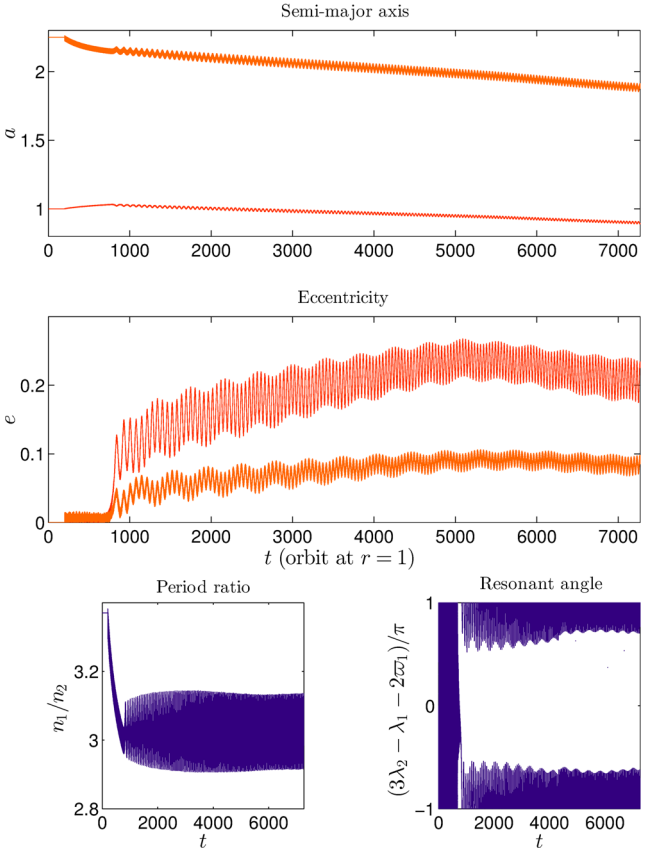

Figure 17. Results for a 2D two-planet run where the outcome is migration in a 3:1 resonance. The parameters were chosen to correspond to the HD 60532 system (see text), with the outer planet starting at $r = 2.25$. The panels correspond to those in Fig. 4 except that the resonant angle plotted is $3\lambda_2 - \lambda_1 - 2\varpi_1$.

In addition, the grid outer boundary was shifted from 3.75 to 4.4 such that it was kept distant enough from the outermost planet. Bearing in mind the observational uncertainties, the mass ratio being larger for the outer planet in this system allows it to potentially resemble the HD 6805 system. This run attains a 2:1 resonance and migrates inwards with the two resonant angles ultimately librating around zero and such that $-r/\dot{r} \sim 10^5$ inner planet initial orbital periods. This characteristic time is close to that found for the standard run and so a very similar discussion will follow (see Section 5).

4.6 The formation of a 3:1 resonance

We have also studied a case with planet masses chosen to correspond to the HD 60532 system (see Table 1) where the planets have been found to be in a 3:1 resonance (see Laskar & Correia 2009).

The results of the simulations are shown in Fig. 17. The quantities plotted in the different panels correspond to those in Fig. 4 except that the right lowermost panel shows the resonant angle $3\lambda_2 - \lambda_1 - 2\varpi_1$. This is found to exhibit large-amplitude librations about π as does the angle $3\lambda_2 - \lambda_1 - 2\varpi_2$. The behaviour of the angles that we find here is similar to that presented by Laskar & Correia (2009). Note that the two planets speed up their joint inward migration slightly between $t = 5000$ and 7000 while their mean eccentricities decrease slightly. As the rate of growth of eccentricity increases with the rate of convergent migration as the planets become closer to resonance (e.g. Papaloizou 2003; Baruteau & Papaloizou 2013), this is an indication that the planets are tending to converge more slowly rather than there being an increase in the damping rate of their eccentricities. That in turn can be traced to a tendency of the inner planet to increase its rate of migration inwards at late times unlike in most other 2D cases where an inner planet is pushed by an outer planet. Note that in this case the difference is that the inner planet is more massive and so more effective at clearing away the inner disc which opposes its inward migration.

We remark that this system has been considered by Sándor & Kley (2010). They considered a disc with the same aspect ratio and approximately the same mass interior to the inner planet as considered here. However, the viscosity parameter $\alpha = 0.01$ throughout corresponding to a much larger viscosity than we consider for our standard model disc. They found that the planets attained a 3:1 resonant configuration with $-r/\dot{r} \sim 4500$ orbits. In our case, this time is extended to 60 000 initial inner planet orbits. This is discussed further below.

5 SUMMARY AND DISCUSSION

In this paper, we have performed 2D and 3D simulations of pairs of giant planets that have attained a mean motion resonance in a protoplanetary disc. We considered disc models both with an inner active region and an outer inactive region with lower effective viscosity as well as disc models incorporating only one of these regions. Different magnitudes for the viscosity in both regions were considered. This was found to have only minor effects on the results as long as the surface density was scaled such as to maintain the

same steady-state accretion rate – or equivalently, outward directed angular momentum flux, and this scaling did not result in the surface density becoming so small that the planet mass dominated its local neighbourhood. Disc models with a range of masses corresponding to a range of accretion rates were considered, the smallest corresponding to the late stages of the protoplanetary disc lifetime. Simulations were run for up to 20 000 initial orbits of the inner planet.

5.1 Maintenance of a 2:1 commensurability

When the mass ratio for both planets was 10^{-3}, a 2:1 commensurability was maintained for small enough disc masses. For our standard case with a low-mass disc and a corresponding steady-state accretion rate of 6×10^{-10} $M_\odot$ yr^{-1}, the inward migration time $-r/\dot{r} \sim 1.5 \times 10^5$ inner planet initial orbital periods is a characteristic viscous time-scale and so corresponds to standard type II migration.

Noting that observed parameters are somewhat uncertain, those for this model may approximately correspond to those for HD 155358 and 24 Sextantis (see Table 1) if the inner planet semi-major axis is respectively taken to be 0.64 and 1.33 au, respectively. The inward migration times are then respectively $\sim 0.77 \times 10^5$ and 2.3×10^5 yr which are relatively short compared to a characteristic protoplanetary disc lifetime. For illustrative purposes, let us assume the planets have migrated in resonance for a time, t, and use the scaling procedure given in Section 3.2 to estimate the initial radius of the inner planet. For either of the two examples, we obtain $r = (t/(1.5 \times 10^5 \text{ yr}))^{2/3}$ au ~ 3.5 au for $t = 10^6$ yr. We note that this is beyond the ice line, with location estimated at about 2.7 au from a solar mass star (see e.g. Martin & Livio 2013). But we emphasize that the scaling used restricts the disc model such that $\Sigma \propto r^{-2}$. While this might be relaxed to some extent, the surface density cannot exceed this projection by a large amount because a commensurability with period ratio closer to unity would be formed (see below).

However, we note that the quoted eccentricity for the inner planet in HD 155358 is 0.17 ± 0.03 (Robertson et al. 2012a). The mean value is exceeded for the standard run at 4000 orbits after going into resonance with the implication that the planets could not have been in resonance longer than this time. If this is the case, the above discussion would have to be modified to allow the planets to migrate independently from larger radii before converging on to resonance close to their final locations. This is likely to need to be considered for different possible exterior disc models and in addition the planets may have built up their masses as they went (see e.g. Tadeu dos Santos et al. 2015). These considerations are beyond the scope of this paper. None the less, because the migration rates for single planets and the resonantly coupled planets are in general similar, the estimated starting radii would also be similar for disc models that are similar to those we considered. But note that the attained eccentricities depend on the eccentricity damping rates which depend on the details of the disc model (see Crida et al. 2008). For example, we found that for the same amount of relative resonant migration, the entirely inactive disc model led to smaller eccentricities while the 3D layered model led to larger eccentricities. Thus, it is important to note that there is uncertainty as to how long the planets could have been in resonance. In the same context, we comment that migration in the completely active disc model was slower by a factor of $\sim$1.6 compared to the standard case on account of its lower mass, that being determined so as to maintain the same steady-state accretion rate as in the standard case. Furthermore, the potential importance of a residual inner gaseous disc for damping the eccentricity of the inner planet and so preventing the eccentricities of both planets from continuing to increase in the later stages of the orbital evolution has been stressed by Crida et al. (2008). In addition, Murray, Paskowitz & Holman (2002) indicate that a residual disc of planetesimals could produce a similar effect.

We undertook 3D simulations that incorporated consideration of the vertical structure of the disc. Both models that adopted a viscosity that was independent of θ and layered models for which a viscosity was only applied in the upper portion of the θ domain were considered. The orbital evolution that was obtained was found to be in good agreement with that obtained from corresponding 2D simulations. One effect seen in the 3D simulations that cannot be recovered from the 2D simulations is the vertical flow towards the mid-plane in the interior neighbourhood of the planet. However, because this occurs in the gap region where the density is very low, this does not lead to significant departures from the 2D results for the orbital evolution.

In order to consider a system resembling the HD 6805 system, we performed a simulation identical to the standard one except that the mass of the outer planet was increased by a factor of 2. This behaved like the standard case with maintenance of a 2:1 commensurability and an inward migration rate $-r/\dot{r} \sim 10^5$ inner planet initial orbital periods. Using the same scaling argument as above, the inner planet can be estimated to start at a radius being $\sim$5.5 au if resonant migration is assumed for $t = 10^6$ yr.

5.2 Increasing planet mass and the formation of a 3:1 resonance

We have also studied a case with planet masses chosen to correspond to the HD 60532 system which has the larger planet mass ratios 2.2×10^{-3} and 5.2×10^{-3} (see Table 1). These planets are observed to be in a 3:1 resonance (Laskar & Correia 2009). In our simulation, the planets attained a 3:1 resonant configuration with $-r/\dot{r} \sim 6 \times 10^4$ initial inner orbits. For the purposes of an illustrative discussion, if we assume that the scaling to larger radii discussed in Section 3.2 applies, we find that if the system arrived in its present location after having undergone inward migration in resonance for 10^6 yr, it should have started with the inner planet at an orbital radius of $\sim$ 7.4 au. For a shorter evolution time of 4×10^5 yr, the corresponding starting location shifts to 4 au. However, note that as the orbital configuration obtained in the simulation is like that observed, the two planets may have only spent a relatively small time in resonance, comparable to our simulation run time of $\sim$ 6000 orbits. In that case, the planets could have migrated independently, starting at initial radii that did not differ by a large factor on account of the single-planet migration rates being comparable. If this is the case, detection of the system in resonance would be unlikely. On the other hand, only one system of this kind is currently known.

5.3 Effect of increasing disc mass

When the surface density or equivalently the steady-state accretion rate was increased, the character of the migration of the resonantly coupled pairs of Jupiter mass planets changed. When it was increased by a factor of 5, the planets are found to enter a 5:3 resonance which became unstable after about 5000 orbits leading to a planet–planet scattering, as was found by Lee et al. (2009) who adopted an N-body approach. The unstable character of the 5:3

resonance makes the observed occurrence of such a resonance less likely than a 2:1 resonance.

If pairs of planets formed at a few au and then migrated to their present locations with the inner planet being at around 1 au (such as for the HD 155358 and 24 Sextantis systems) while maintaining a 2:1 commensurability for a characteristic time comparable to the disc lifetime, the disc should have a low mass as might occur during the later stages of a protoplanatary disc lifetime. We have found that a disc with significantly larger mass produces an unstable 5:3 resonance resulting in its observed occurrence being less likely. Although 3:2 resonances may be produced in other situations (e.g. Rein et al. 2010, and see the end of Section 4.3 above), characteristic evolution times are again short.

Finally, consideration of systems containing a pair of giant planets with the innermost one being significantly more massive, for which the mechanism outlined by Masset & Snellgrove (2001) may operate more efficiently, should be undertaken but is beyond the scope of this paper. A recently discovered system of this kind is HD 204313 (Robertson et al. 2012b). This contains an inner planet of mass $3.55\,M_{\rm J}$ with semi-major axis 3.04 au and an outer planet of mass $1.68\,M_{\rm J}$ with semi-major axis 3.93 au, the pair being in or close to a 3:2 commensurability. Accordingly, this will be the focus of a future study.

ACKNOWLEDGEMENTS

We thank the anonymous referee for useful comments and suggestions which greatly enhanced the quality of this paper. QA was supported by ENS Cachan and thanks warmly DAMTP, University of Cambridge for their hospitality.

REFERENCES

Balbus S. A., Hawley J. F., 1991, ApJ, 376, 214
Baruteau C., Papaloizou J. C. B., 2013, ApJ, 778, 7
Baruteau C. et al., 2014, Protostars and Planets VI. Univ. Arizona Press, Tucson, p. 667
Beauge C., Ferraz-Mello S., Michtchenko T. A., 2012, Res. Astron. Astrophys., 12, 1044
Bryden G., Chen X., Lin D. N. C., Nelson R. P., Papaloizou J. C. B., 1999, ApJ, 514, 344
Calvet N., Muzerolle J., Briceño C., Hernandez J., Hartmann L., Saucedo J. L., Gordon K. D., 2004, AJ, 128, 1294
Correia A. C. M. et al., 2009, A&A, 496, 521
Crida A., Sándor Z., Kley W., 2008, A&A, 483, 325
Crida A., Baruteau C., Kley W., Masset F., 2009a, A&A, 502, 679
Crida A., Masset F., Morbidelli A., 2009b, ApJ, 705, 148
de Val-Borro M., Artymowicz P., D' Angelo G., Peplinski A., 2007, A&A, 471, 1043
Emelyanenko V., 2012, Sol. Syst. Res., 46, 321
Gammie C. F., 1996, ApJ, 457, 355
Ivanov P. B., Papaloizou J. C. B., Polnarev A. G., 1999, MNRAS, 307, 79
Johnson J. A. et al., 2011, AJ, 141, 16
Kley W., 1999, A&A, 208, 98
Kley W., Lee M. H., Murray N., Peale S. J., 2005, A&A, 437, 727
Kley W., Bitsch B., Klahr H., 2009, A&A, 506, 971
Laskar J., Correia A. C. M., 2009, A&A, 596, 5
Latter H. N., Balbus S., 2012, MNRAS, 424, 1977
Lee M. H., Peale S. J., 2002, ApJ, 567, 596
Lee A. T., Thommes E. W., Rasio F. A., 2009, ApJ, 691, 1684
Lin D. N. C., Papaloizou J. C. B., 1986, ApJ, 309, 846
Lin D. N. C., Papaloizou J. C. B., 1993, in Levy E. H., Lunine J. I., eds, Protostars and Planets III, p. 749
Martin R. G., Livio M., 2013, MNRAS, 428, L11
Masset F. S., 2000, A&A, 141, 165
Masset F., Snellgrove M., 2001, MNRAS, 320, L55
Mignone A., Bodo G., Massaglia S., Matsakos T., Tesileanu O., Zanni C., Ferrari A., 2007, ApJS, 170, 228
Mignone A., Flock M., Stute M., Kolb S. M., Muscianisi G., 2012, A&A, 545, A152
Mihalas D., Weibel Mihalas B., 1984, Foundations of Radiation Hydrodynamics. Oxford Univ. Press, New York
Murray N., Paskowitz M., Holman M., 2002, ApJ, 565, 608
Nelson R. P., Papaloizou J. C. B., Masset F., Kley W., 2000, MNRAS, 318, 18
Nelson R. P., Papaloizou J. C. B., 2002, MNRAS, 333, 26
Nelson R. P., Gressel O., Umurhan O. M., 2013, MNRAS, 435, 2610
Pierens A., Nelson R. P., 2010, A&A, 520, id.A14
Rein H., Papaloizou J. C. B., Kley W., 2010, A&A, 510, A4
Papaloizou J. C. B., 2003, Celest. Mech. Dyn. Astron., 87, 53
Rein H., Payne M. J., Veras D., Ford E. B., 2012, MNRAS, 426, 187
Robertson P. et al., 2012a, ApJ, 749, 39
Robertson P. et al., 2012b, ApJ, 754, 50
Sándor Z., Kley W., 2010, A&A, 517, 31
Shakura N. I., Sunyaev R. A., 1973, A&A, 24, 337
Snellgrove M. D., Papaloizou J. C. B., Nelson R. P., 2001, A&A, 374, 1092
Tadeu dos Santos M., Correa-Otto J. A., Michtchenko T. A., Ferraz-Mello S., 2015, A&A, 573, A94
Trifonov T., Reffert S., Tan X., Lee M. H., Quirrenbach A., 2014, A&A, 568, A64
Uribe A. L., Klahr H., Henning T., 2013, ApJ, 769, 97
Wright J. T. et al., 2011, ApJ, 730, 93

This paper has been typeset from a TEX/LATEX file prepared by the author.